# Inelastic and elastic processes in the transmission of $F^+$, $F^-$, and $F_2^-$ from $PF_3$/Ru(0001) through thin rare-gas films

N. J. Sack,* M. Akbulut, and T. E. Madey†
*Department of Physics and Astronomy, and Laboratory for Surface Modification, Rutgers, The State University of New Jersey, Piscataway, New Jersey 08855*

P. Klein and H. M. Urbassek
*Fachbereich Physik, Universität Kaiserslautern, Erwin-Schrödinger-Straße, D-67663 Kaiserslautern, Germany*

M. Vicanek
*Institut für Theoretische Physik, Technische Universität Braunschweig, Postfach 3329, D-38023 Braunschweig, Germany*
(Received 22 June 1995; revised manuscript received 15 February 1996)

We have studied the transmission of low-energy (<10 eV) $F^+$, $F^-$, and $F_2^-$ ions through ultrathin Kr and Xe films. The ions are produced by electron-stimulated desorption from a $PF_3$-covered Ru(0001) surface at 25 K, and their yields and angular distributions are measured with a digital, angle-resolving ion detector. The rare-gas films are condensed onto the $PF_3$ layer, and the yield and angular distribution of the ions are measured as a function of the rare-gas film thickness. We find that $F^+$ ions are attenuated nearly completely by ~1 ML of Kr or Xe, and attribute this to both one-electron charge transfer and elastic scattering. Surprisingly, we find an increase in $F^-$ yield for the first rare-gas layer with respect to the clean surface value, which is accompanied by a dramatic change in the ion angular distribution. The $F^-$ yield decreases to zero around 2.5 ML Kr or Xe; we explain the $F^-$ attenuation and the change in the $F^-$ angular distributions in an elastic-scattering model. The increase in yield is attributed to a reduction in the neutralization probability of $F^-$ with the surface in the presence of the rare-gas layer. [S0163-1829(96)06432-6]

## I. INTRODUCTION

The interaction of low-energy (<10 eV) ions with solids is of physical interest due to the wealth of phenomena that all occur in this collision energy regime, such as elastic-scattering, charge transfer, or ion-molecule reactions.[1] The relative importance of these scattering processes is strongly dependent on the electronic characteristics of both the ion and the solid.[2,3]

Transport of ions with energy <10 eV through thin films plays an important role in determining the depth of origin of secondary ions desorbing from surfaces under electron or photon bombardment.[4–8] The secondary ions usually have an energy of a few eV. If they are generated below the surface, their escape probability from the surface is determined by their interaction with the surface layers of the solid.

To study the interaction of low-energy ions with solids, we have chosen the following experimental approach:[9] We generate the ions by electron-stimulated desorption (ESD) from a substrate that emits secondary ions under electron bombardment. We measure the yield, energy distribution, and angular distribution of the ions with a two-dimensional digital ion detector. We condense overlayers ranging in thickness from a fractional monolayer to several monolayers on top of the ESD active surface, and monitor the ion yield, energy, and angular distribution as a function of overlayer thickness. From these data we draw conclusions about the interaction of the ions with the thin films.

In our first study we have found that 7-eV oxygen ions can penetrate Kr or Xe overlayer films several monolayers thick.[9,10] We attribute the attenuation to elastic scattering, and suggest that the large mean free path of the oxygen ions in the rare-gas overlayers is caused by the fact that the repulsive part of the $O^+$ rare-gas interaction potential occurs at a surprisingly small internuclear distance compared to the nearest-neighbor distance in the rare-gas solid, so that $O^+$ can ''channel'' through the rare-gas film. Molecular-dynamics simulations based on elastic scattering by Klein, Vicanek, and Urbassek[11] are consistent with our experimental data for Kr and Xe. Ar was found to attenuate the $O^+$ stronger than the simulation predicted.

On the other hand, we have observed strong attenuation of $O^+$ in $H_2O$ overlayers: about 0.5 ML of water is enough to suppress the $O^+$ signal nearly completely.[12] We interpret the results to indicate charge-exchange processes between $O^+$ and $H_2O$; the same mechanism was suggested for the attenuation of $O^+$ in $NH_3$.[12,13]

Recently we reported on a study on the transmission of negative ions through ultrathin Xe films.[14] We find that the yield of $F^-$ from $PF_3$/Ru(0001) increases upon adsorption of 1 ML of Xe, and we have suggested that the increase may be due to a reduction of the neutralization probability of the surface induced by the Xe overlayer.

Here we present results on the transmission of $F^+$, $F^-$, and $F_2^-$ through thin films of Kr or Xe. The ions are desorbed by electron stimulated desorption from 1 ML of $PF_3$ on Ru(0001). Whereas $F^+$ and $F_2^-$ are suppressed by a Kr or Xe overlayer 1 ML thick, we find that 1 ML of Kr or Xe *increases* the emission yield of $F^-$ ions. The increase is accompanied by a dramatic change in the angular distribution of $F^-$.

 

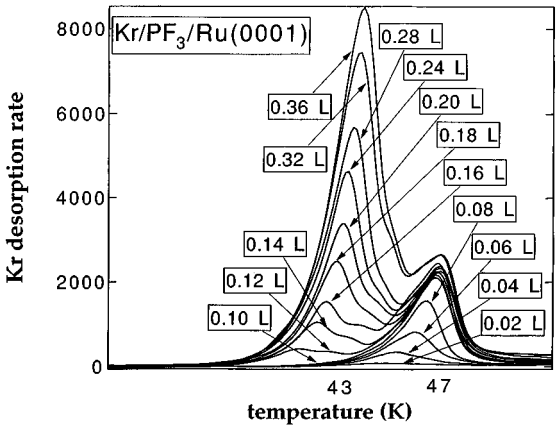


FIG. 1. Thermal-desorption spectra of Kr from a $PF_3$-covered Ru(0001) surface. The exposure is measured with an uncorrected ion gauge. The heating rate is of order 10 K/s.

## II. EXPERIMENTAL DETAILS

The experiments are carried out in an ultrahigh-vacuum chamber that has been described in detail elsewhere.[15] In short, the chamber is equipped with instrumentation to perform Auger electron spectroscopy (AES), low-energy electron diffraction (LEED), thermal-desorption spectroscopy (TDS), and electron-stimulated desorption ion angular distribution (ESDIAD) measurements. For the latter, an electron source provides a focused beam of 300-eV electrons onto the sample, and the ions that desorb from the sample can be detected with a two-dimensional digital ESDIAD detector equipped with time-of-flight capability for mass- and energy-selective ion detection. The electron fluence is kept low, $<2\times10^{13}$ cm$^2$, in order to minimize beam damage to the substrate. The Ru(0001), which can be cooled to 25 K with a closed-cycle helium refrigerator and heated to 1600 K by electron bombardment, is cleaned by sputtering and heating in oxygen and is found to be clean by means of AES and to be well ordered by means of LEED. A saturation coverage of $PF_3$ (one $PF_3$ molecule per three Ru atoms) is dosed onto the surface at 100 K, subsequently, it is annealed at 270 K for a few seconds, after which the surface exhibits a $(\sqrt{3}\times\sqrt{3})R30°$ LEED pattern and azimuthally ordered $F^+$ and $F^-$ ESDIAD patterns.[16] All ESDIAD measurements are performed at 25 K. Kr or Xe is dosed at 25 K through a separate doser, and the coverage is determined by TDS. As an example, in Fig. 1 we show TDS spectra of Kr desorbing from $PF_3$/Ru(0001). The exposure is measured with an uncalibrated Bayard Alpert ion gauge, and is not corrected for the dosing geometry. Two peaks are seen, one at 43 K and one at 47 K. The high-temperature peak saturates at a nominal exposure of 0.10 L, which is also the exposure necessary to complete 1 ML of Kr on clean Ru(0001) measured under our dosing conditions (see also Ref. 17). We attribute this peak to desorption from the Kr monolayer on $PF_3$ Ru(0001). The low-temperature peak continues to grow with increasing exposure, and is attributed to multilayer desorption. We conclude from TDS that the first layer of Kr is completed before the second layer starts to grow. A similar coverage calibration has also been performed for Xe. We estimate the uncertainty in the coverage calibration to be of order 10%.

## III. RESULTS

### A. ESD ion desorption from 1-ML $PF_3$Ru/(0001)

Electron bombardment of 1-ML $PF_3$/Ru(0001) leads to desorption of $F^+$, $F^-$, and $F_2^-$. We perform the experiments using a primary electron energy of 300 eV and a total electron fluence of order $10^{13}$ cm$^{-2}$. In Figs. 2(a)–2(c), show the ESDIAD patterns and contour plots of the three ions $F^+$, $F^-$, and $F_2^-$. The ions desorb with a hexagonal array of trajectories from the surface. The $F_2^-$ pattern is less clearly resolved, but it exhibits also a hexagonal structure in the azimuthal distribution.

Part of this study is to investigate the attenuation of normal vs off-normal ESD ion beams by overlayers. Therefore, for the study of $F^+$ through rare gases we use an electron-beam-damaged $PF_3$ surface as a substrate. Bombardment of 1 ML of $PF_3$ with high fluences of electrons (here $\sim10^{16}$ cm$^{-2}$) leads to dissociation of $PF_3$ into $PF_2$ and PF.[18] Both $PF_2$ and PF give rise to $F^+$ desorption under electron bombardment, but no $F^-$ or $F_2^-$ are detected from the dissociation products. Due to their adsorption geometry, $PF_2$ leads to $F^+$ emission with a hexagonal array of trajectories very similar to that of $F^+$ from $PF_3$. However, ESD from PF yields a strong $F^+$ beam centered on the surface normal, because the P-F bond is oriented along the surface normal. In Fig. 2(d) we show the ESDIAD pattern and contour plot of $F^+$ from this surface.

### B. $F^+$ transmission through Kr and Xe

In Fig. 3(a) we depict the attenuation by Kr overlayers of $F^+$ from an electron-beam-damaged $PF_3$ monolayer on Ru(0001). The filled circles refer to the total, angle-integrated $F^+$ yield, the open circles to the integrated counts found in the center peak (normal emission), and the triangles to the integrated intensity of one (representative) off-normal beam. (Note that all yields are normalized to 1 for the surface with zero coverage of rare gas.) It can be seen that 1 ML of Kr suppresses the $F^+$ signal nearly completely. The off-normal beam is attenuated at a slightly higher rate than the normal beam.

Figure 3(b) shows the same plot for Xe as an overlayer. The noise in the data is smaller due to more reproducible dosing conditions of Xe as compared to Kr. The attenuation and the difference in attenuation between normal and off-normal beams are similar to the results shown for Kr.

In Fig. 3(c) we compare the attenuation of the center $F^+$ yield by Kr and Xe on a linear plot. Using the slopes of the straight lines in Fig. 3(c) and the estimated number density[11] of $\sim7.2\times10^{14}$ atoms/cm$^2$ for Kr and $\sim6.1\times10^{14}$ atoms/cm$^2$ for Xe, we derive attenuation cross sections of $\sim(1.4\pm0.4)\times10^{-15}$ cm$^2$ for Kr and $\sim(2.2\pm0.6)\times10^{-15}$ cm$^2$ for Xe. From the measured $F^+$ attenuation cross sections for Kr and Xe, we can estimate the attenuation collision radius ($R$) of $\sim$2.1 Å for Kr and $\sim$2.6 Å for Xe; for comparison, the crystal atomic radii of Kr and Xe are 1.9 and 2.2 Å, respectively. (Note that the data scatter about the linear fits; we derive the cross sections here to compare them with attenuation data for $F^-$ and $F_2^-$, as described in Sec. III C and III D below. Also, see Sec. IV C for a discussion of our attenuation model.)

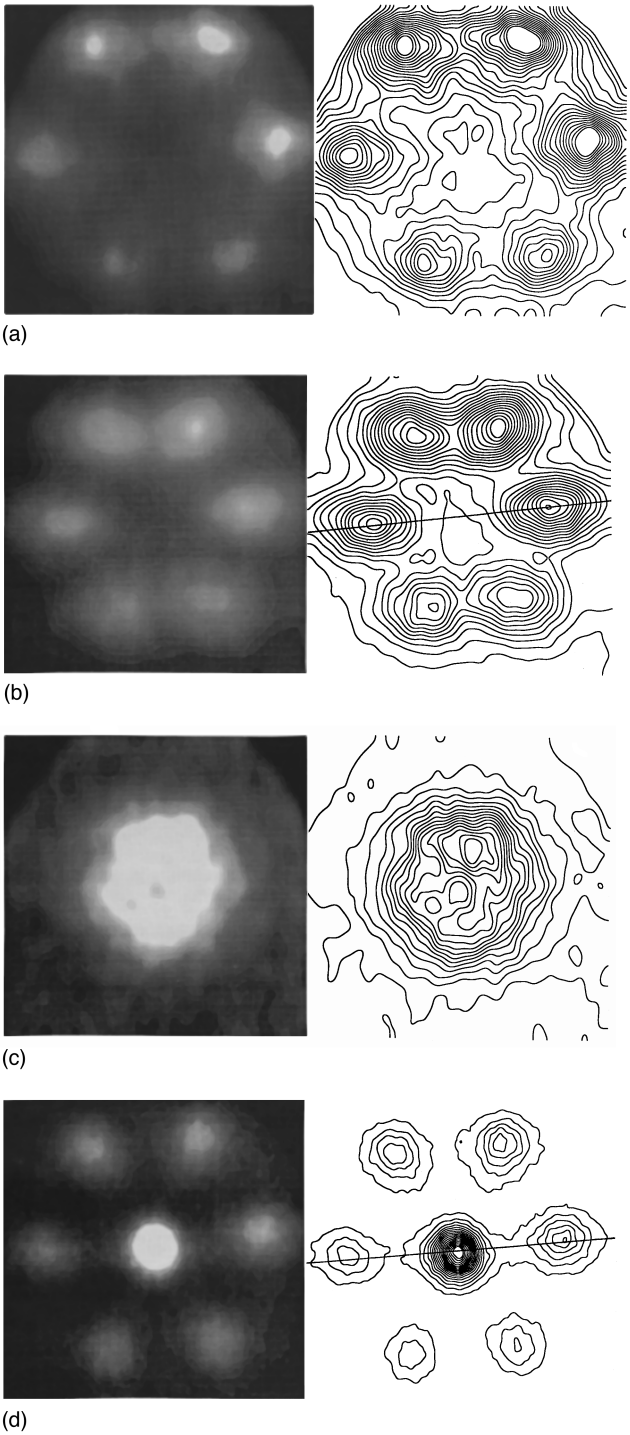


FIG. 2. ESDIAD patterns and contour plots obtained from $PF_3$/Ru(0001) (a) for $F^+$ with a sample bias of +200 V; (b) for $F^-$ with a sample bias of −140 V; (c) for $F_2^-$ with a sample bias of −140 V; and (d) for $F^+$ from electron-beam-damaged $PF_3$ (see text). The asymmetries between the top and bottom of the plot are of a technical nature. The lines in 2(b) and 2(d) indicate the direction of the profiles shown in Figs. 5(c) and 4.

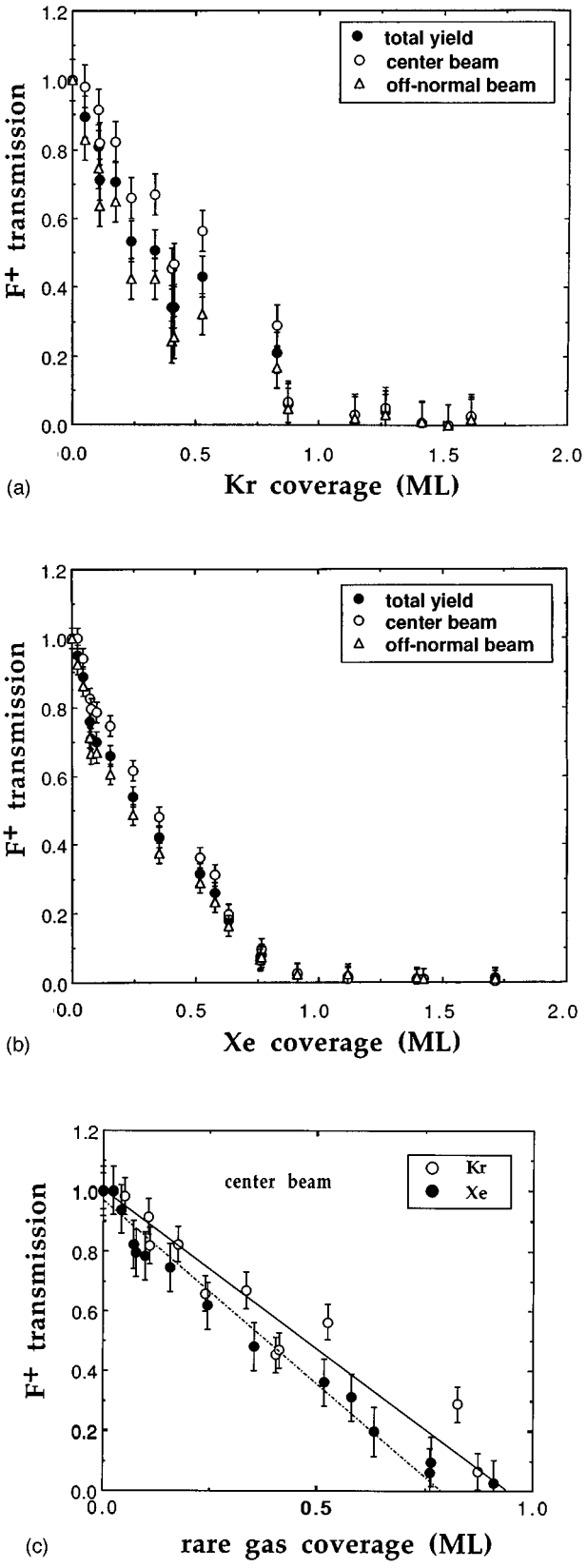


FIG. 3. $F^+$ yield obtained from $PF_3$/Ru(0001) as a function of rare-gas overlayer thickness; (a) for Kr; (b) for Xe. Shown are the total angle- and energy-integrated yield, the yield of the center peak, and the yield of one off-normal beam. The data are normalized to unity for the clean surface value. (c) Plot of the center $F^+$ yield as a function of Kr and Xe overlayer coverage.

In Fig. 4 we illustrate details of the change in the angular distribution of $F^+$ with increasing Xe coverage. We show profiles of the $F^+$ desorption beam, cut through the center beam, and two off-normal beams, along the line indicated in Fig. 2(d). The data are normalized to unity at their maximum. Note that for coverages below ~0.57 ML of Xe, there

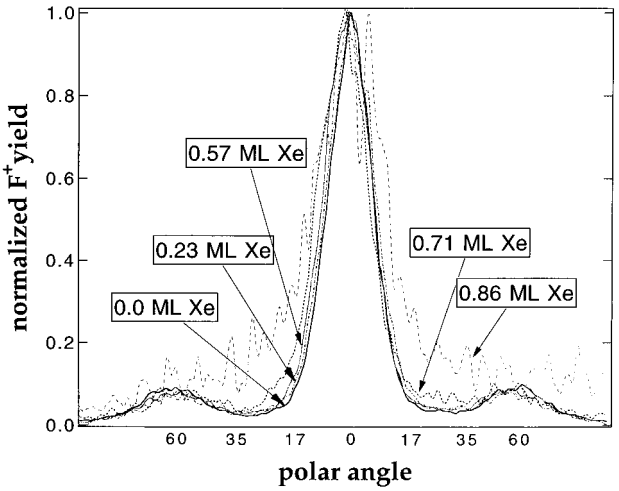


FIG. 4. Cut through the $F^+$ ESDIAD pattern through the center spot and through two off-normal beams along the line in Fig. 2(d), as a function of Xe coverage. The data are normalized to unity at their maximum.

is little or no detectable change in the $F^+$ beam profiles. However, for coverages above 0.7 ML the normal and off-normal beams are less clearly separated than for lower coverages. This may indicate a small contribution of large angle scattering. However, large angle scattering of $F^+$ is by far less obvious than large angle scattering of $F^-$, as discussed in Sec. III C.

### C. $F^-$ transmission through Kr and Xe

We find a dramatic change in the $F^-$ ion angular distribution with increasing rare-gas coverage. Figure 5(a) depicts an ESDIAD pattern and contour plot of $F^-$ ESD from 0.25 ML Xe on 1-ML $PF_3$Ru(0001). Superimposed on the original pattern of hexagonal beams [Fig. 2(b)], a broad emission centered on the surface normal can be seen. Similar data are observed for Kr overlayers. We decompose the hexagonal and the broad normal contributions in the following way: We subtract a multiple $k$ of the clean surface pattern $P_0$ (hexagonal contribution) from the ESDIAD pattern $P$ in such a way that we obtain a spectrum of cylindrical symmetry, $P_{\mathrm{bn}}$ (broad normal $F^-$ contribution) depicted in Fig. 5(b):

$$P_{\mathrm{bn}} = P - kP_0 . \tag{1}$$

The change in angular distribution is further illustrated in Fig. 5(c) by the $F^-$ ion beam profiles, cut along the line indicated in Fig. 2(b).

The change in the ion angular distribution is accompanied by an increase in the yield of $F^-$ with increasing rare-gas coverage. For Kr, in Fig. 6 we show the total $F^-$ yield and the contributions from one hexagonal beam (from pattern $kP_0$) and from the broad normal beam ($P_{\mathrm{bn}}$) which we obtain by subtraction according to Eq. (1). The total yield (normalized to unity for 0 ML Kr coverage) exhibits a maximum between 0.5 and 1.0 ML Kr, and decreases to 0 at around 2.5 ML. The hexagonal contribution increases with Kr coverage at low coverage, has a maximum around 0.3 ML, and decreases to zero around 1.5 ML. The broad normal emission (which is initially close to zero) has a maximum around 1

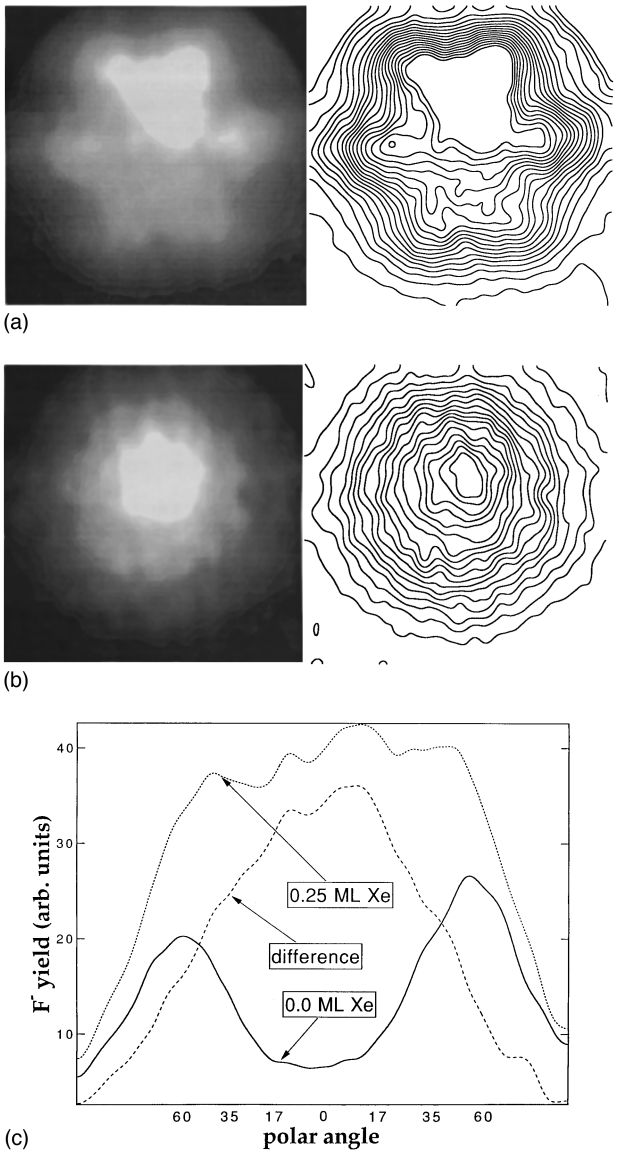


FIG. 5. (a) $F^-$ ESDIAD patterns and contour plots obtained from 0.25-ML Xe adsorbed on $PF_3$/Ru(0001) measured with a sample bias of $-140$ V. (b) Same pattern after subtraction of two times the clean surface spectrum [Fig. 2(b)]. The asymmetries between the top and bottom of the plot are of a technical nature. (c) Cut through the $F^-$ ESDIAD pattern for the clean $PF_3$ surface, for 0.25-ML Xe adsorbed on $PF_3$/Ru(0001), and for the difference spectrum (5b); cuts are along the line indicated in Fig. 2(b). Note that the angle scale is nonlinear due to field compression of the ion beam.

ML Kr and decreases to 0 around 2.5 ML. The data for Xe overlayers have been published previously:[14] A change in angular distribution similar to Fig. 6 is observed, along with an increase in the total intensity by a factor 4; the maximum in the total intensity occurs between 0.5 and 1.0 ML Xe.

Figure 7(a) shows the total $F^-$ yield as a function of rare-gas coverage for Kr and Xe on a linear plot. (Note that the data are normalized to unity for the clean surface value.) The maximum enhancement value of the $F^-$ yield is $\sim$4 for Xe and $\sim$2.5 for Kr overlayers. Figure 7(b) shows the same data normalized to unity at 1 ML in order to derive $F^-$ attenuation cross sections between 1 and 2 ML. The lines in Fig. 7(b)

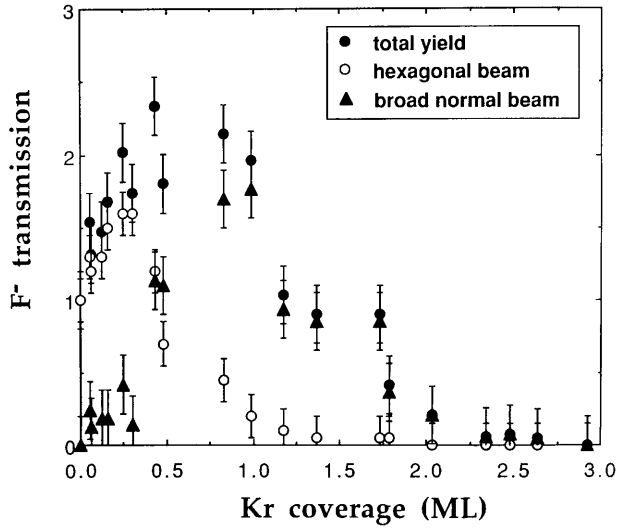


FIG. 6. (a) Total angle- and energy-integrated $F^-$ yield (filled circles) obtained from $PF_3$/Ru(0001) as a function of Kr overlayer coverage. The data are normalized to 1 for the clean surface value. Open circles: yield in hexagonal spots; triangles: yield in broad normal-emission spot.

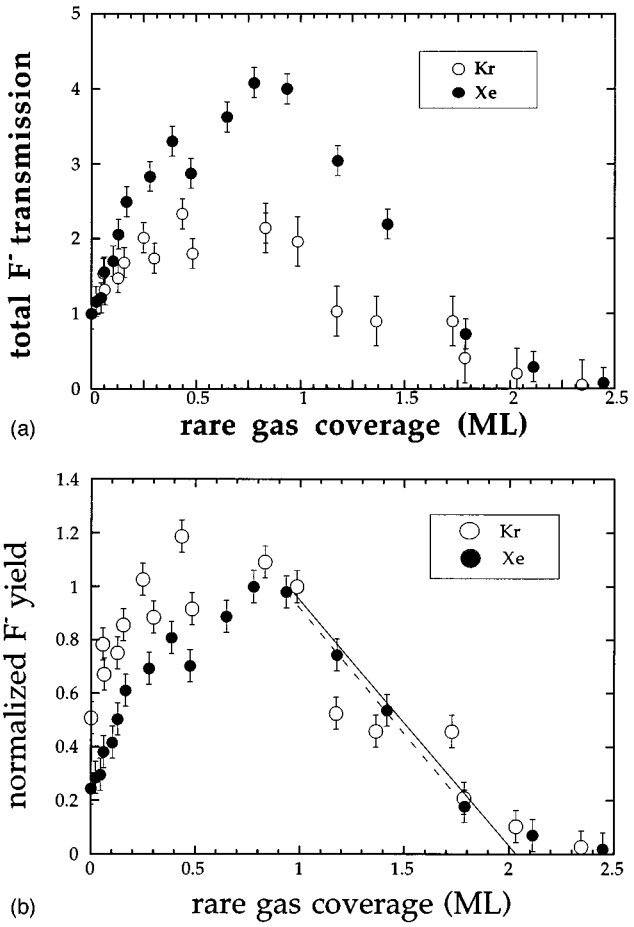


FIG. 7. Linear plot of the total angle- and energy-integrated $F^-$ yield obtained from $PF_3$/Ru(0001) as a function of Kr and Xe overlayer coverage. The data are normalized to unity (a) for the clean surface value and (b) at 1 ML.

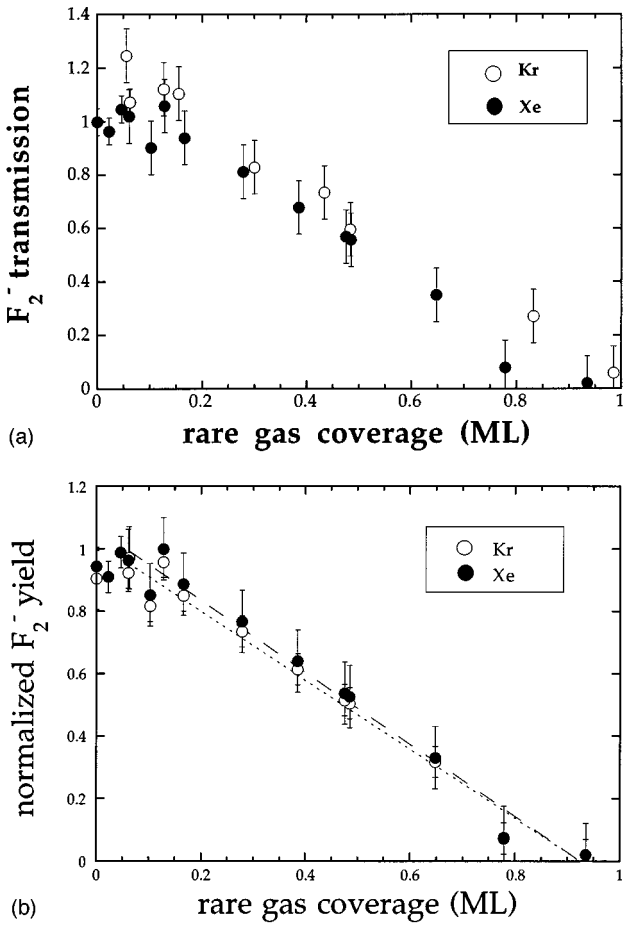


FIG. 8. Total angle-integrated $F_2^-$ yield as a function of Kr and Xe overlayer coverage. The data are normalized to unity (a) for the clean surface value and (b) at 1 ML.

represent linear fits. From the slopes of the straight lines in Fig. 7(b), and based on the monolayer number densities for Kr and Xe (Sec. III B), we derive the cross sections to be $\sim(1.1\pm0.6)\times10^{-15}$ cm$^2$ for Kr and $\sim(1.5\pm0.4)\times10^{-15}$ cm$^2$ for Xe.

### D. $F_2^-$ transmission through Kr and Xe

The total, angle-integrated yield of $F_2^-$ is depicted in Fig. 8(a) as a function of Kr and Xe overlayer coverage. There seems to be a slight increase in the yield with coverage at coverages $<0.15$ ML; above 0.15 ML, the $F_2^-$ yield decreases with increasing coverage, and reaches a value of 0 around 1 ML.

Figure 8(b) shows the normalized $F_2^-$ yield as a function of rare-gas Kr and Xe thickness. From the slopes of the lines in Fig. 8(b), we derive the cross sections to be $\sim(1.5\pm0.4)\times10^{-15}$ cm$^2$ for Kr and $\sim(1.9\pm5)\times10^{15}$ cm$^2$ for Xe. There is no strong difference in attenuation of $F_2^-$ for Kr overlayers as compared to Xe. It is interesting to note that 1 ML of Kr or Xe is enough to suppress the $F_2^-$ yield nearly completely, while more than 2 ML of Kr or Xe are necessary for equivalent attenuation of the $F^-$ yield. Moreover, the attenuation of $F_2^-$ in Kr (Xe) in the coverage range 0–1 ML is slightly stronger than the attenuation of the $F^-$ yield in the coverage range 1–2 ML. This observation may be correlated

to the structure of the rare-gas films. The rare-gas films are believed to grow with fcc(111) orientation in *A-B-C* fashion (see Sec. IV B for more detail); after completion of the first layer, there are channels perpendicular to the surface normal through which the desorbing ions can escape. After completion of the second layer, there are still some channels normal to the surface. However, the channel size is much smaller than the ionic diameter of $F^-$ (~2.7 Å). Therefore, we expect that the second Kr (Xe) layer attenuates the desorbing $F^-$ ions much more effectively than the first Kr (Xe) layer: the attenuation of the $F^-$ and $F_2^-$ yields depends on the rare-gas film thickness. An important factor in the strong attenuation of $F_2^-$ by Kr (Xe) may be the fact that the ionic diameter of $F_2^-$ (>3.7 Å) (Ref. 19) is larger than the channel size after completion of the first layer.

### E. Secondary electron emission and work-function measurements

There are two main reasons why we are interested in the secondary electron emission from and the work function of the $PF_3$ layer in the absence and the presence of rare-gas overlayers: (i) As we discuss in Sec. IV A, the $F^-$ desorption yield can depend on the secondary electron yield; and (ii) it has been shown previously that the desorption yield can depend on the work function.[20]

In Fig. 9(a) we depict the secondary electron emission energy distributions under the impact of primary electrons from clean Ru, 1 ML $PF_3$/Ru, and 1 ML $PF_3$/Ru covered with various amounts of Kr [Fig. 9(b) shows the data corresponding to the equivalent measurement for Xe]. The primary electron energy is 3.0 keV, and the secondary electrons are measured with a hemispherical energy analyzer. We observe a larger integrated secondary, electron emission yield from 1 ML $PF_3$/Ru than from clean Ru. For both Kr and Xe we observe no significant increase in the secondary electron yield upon adsorption of 1 ML of rare gas; adsorption of 2 ML or more of Kr or Xe leads to an increase in the low-energy secondary electron yield.

From the low-energy cutoff of the secondary electron emission, we can estimate changes in the work function: We assume a work function of clean Ru of 5.52 eV.[20] Adsorption of $PF_3$ leads to an increase in the work function by ~0.4 eV. Both Kr and Xe adsorption on $PF_3$/Ru lead to a decrease in the work function by ~0.07 eV per rare-gas ML.

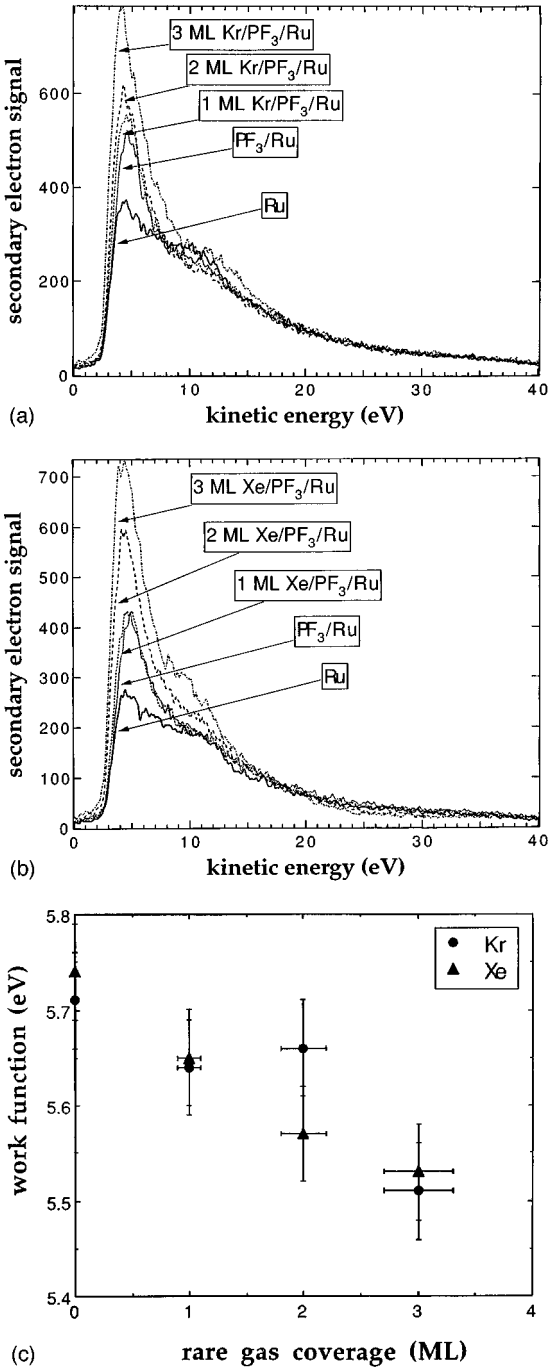


FIG. 9. (a) Secondary-electron emission from Ru(0001), 1-ML $PF_3$/Ru(0001), and in the presence of Kr overlayers, under impact of primary electrons with 3.0-keV energy. The data are not corrected for the work function of the electron energy analyzer. (b) Same measurement for Xe as the overlayer. (c) Changes in the work function as a function of rare-gas overlayer thickness, as derived from the onset energy of the secondary electron emission. We assume a work function of 5.52 eV for clean Ru, (Ref. 20).

## IV. DISCUSSION

### A. ESD processes and electron transport through rare-gas films

#### *ESD of $F^+$, $F^-$, and $F_2^-$ from $PF_3$/Ru(0001)*

Very recently, Akbulut *et al.*[21] have investigated ESD mechanisms of positive and negative ions from $PF_3$ adsorbed on a Pt surface. Since the bonding interaction of $PF_3$ with a Pt surface is similar to the bonding interaction of $PF_3$ with a Ru surface, we believe that the ESD mechanisms observed from a $PF_3$ chemisorbed Pt surface should be similar to those found for $PF_3$ chemisorbed on Ru. In the following, we briefly discuss the ESD mechanisms that lead to desorption of $F^+$, $F^-$, and $F_2^-$ ions from chemisorbed $PF_3$.

The $F^+$ desorption produced by electron bombardment of 1 ML $PF_3$/Pt has a threshold at ~27 eV, which is believed to be due to excitation from the F 2*s* level to the Fermi level of the substrate. This initial ionization event leads to a repulsive state which induces nuclear motion of $F^+$:

$$PF_3 + e^- \rightarrow (PF_3)^+ + 2e^- \rightarrow F^+ + PF_2 + 2e^-. \qquad (2)$$

The mean kinetic energy of the $F^+$ ions is ~4 eV, independent of electron energies in the energy range 40–175 eV.[21]

Electron-stimulated desorption of $F^-$ ions by low-energy electrons occurs through either dissociative attachment (DA) or through dipolar dissociation (DD):

$$\text{DD:}\quad PF_3 + e^- \rightarrow (PF_3)^* + e^- \rightarrow PF_2^+ + F^- + e^-, \quad (3)$$

$$\text{DA:}\quad PF_3 + e^- \rightarrow (PF_3)^{*-} \rightarrow F^- + PF_2. \quad (4)$$

The measurements from the 1-ML $PF_3$/Pt surface have revealed that the $F^-$ ions produced in the electron energy range 0–15 eV originate via DA; the $F^-$ yield exhibits a peak around 11.5 eV.[21] At electron energies above ~15 eV, the $F^-$ yield is mainly produced by DD (ion-pair formation). The $F^-$ ions generated via a DA process with 11.5-eV electrons desorb with a peak kinetic energy of ~0.7 eV, while the $F^-$ ions produced as a result of DD processes (175-eV electron bombardment) desorb with a peak energy of ~1.2 eV.

The $F_2^-$ ions produced from the $PF_3$/Pt surface in the electron energy range 0–15 eV proceed via a DA process:

$$PF_3 + e^- \rightarrow (PF_3)^{*-} \rightarrow F_2^- + PF. \quad (5)$$

The $F_2^-$ yield from a 1-ML $PF_3$ adsorbed Pt surface has an onset at ~9 eV and a peak at ~11.5 eV. At an electron energy above ~15 eV, the $F_2^-$ ions are mainly formed via a DD process:

$$PF_3 + e^- \rightarrow (PF_3)^* + e^- \rightarrow F_2^- + PF^+ + e^-. \quad (6)$$

The $F_2^-$ ions produced by 60-eV electrons desorb with a peak energy of~1.0 eV.

In this study, we use 300-eV primary electrons to initiate the ESD of ions from a $PF_3$-covered Ru(0001). Electron bombardment of the $PF_3$/Ru(0001) surface can produce low-energy secondary electrons originating from the metal substrate. Therefore, in our experiment 300-eV primary electrons can initiate reactions (2), (3), and (6), while the low-energy secondary electrons can lead to $F^-$ and $F_2^-$ formation via reactions (4) and (5), respectively.

### *Angular distribution of $F^+$, $F^-$, and $F_2^-$ from $PF_3$/Ru(0001)*

In order to explain the hexagonal ESDIAD patterns (Fig. 2) for $F^+$ and $F^-$ desorption from 1 ML $PF_3$/Ru(0001), in Fig. 10 we illustrate the adsorption geometry of this system. The trajectories of the desorbing ions reflect the orientation of the chemical bonds that are broken in the excitation process.[22] Hence we expect three $F^+$ or $F^-$ ESDIAD beams from the system as depicted. An additional three beams arise from a second $PF_3$ domain on Ru(0001) that is rotated by 60° compared to the one depicted. The angle of the F-F bond to the surface normal of $PF_3$ adsorbed on Ru(0001) is ~60°, and we estimate the polar angle of desorption to be $60 \pm 10°$ for $F^+$.

Since $F_2^-$ is produced via reaction (5) or (6), we might expect a similar hexagonal symmetry in the $F_2^-$ pattern. Two F atoms from one $PF_3$ molecule form an $F_2^-$ ion and desorb closer to the surface normal than $F^+$ or $F^-$ with an azimuthal orientation broken between the two P-F bonds. Since there are several atoms involved in this desorption process, we can expect a much less sharp pattern as compared to the $F^+$ and $F^-$ patterns, in agreement with the observation [Fig. 2(c)].

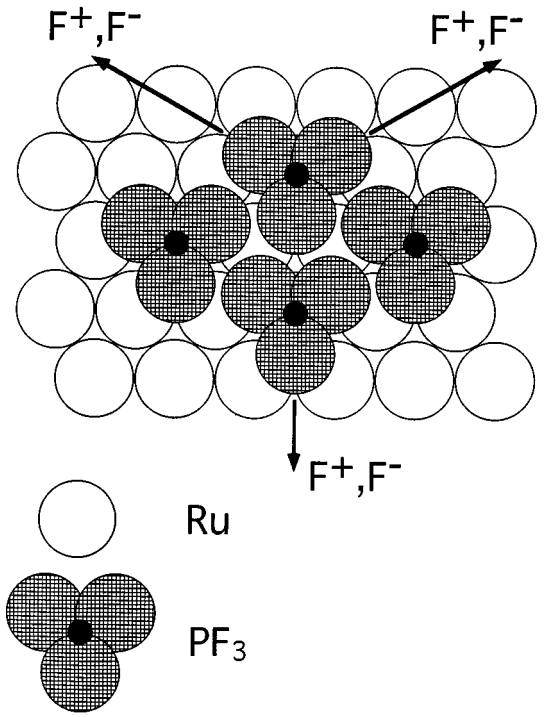


FIG. 10. Geometric ball model for 1-ML $PF_3$/Ru(0001). The arrows indicate the azimuthal direction of $F^+$ and $F^-$ desorption.

### *ESD of $F^+$, $F^-$, and $F_2^-$ from $PF_3$/Ru(0001) in the presence of RG overlayers*

In the presence of a rare-gas overlayer, the primary electron beam has to penetrate the rare-gas film in order to reach the $PF_3$/Ru(0001) substrate. The electrons can cause ionization and electronic excitations in the rare-gas film which can lead to energy loss of the electrons. The gas phase ionization cross sections for rare gases by 300-eV electrons are $2.8\times10^{-16}$ cm$^2$ for Kr and $4\times10^{-16}$ cm$^2$ for Xe,[23] so the electrons do not lose a significant fraction of their energy in the rare-gas overlayers (thickness <5 ML). Because the rates of reactions (2) and (3) are expected not to depend strongly on the primary electron energy around 300 eV, we conclude that the rates of reactions (2) and (3) are not affected strongly by primary electron energy losses in the ultrathin rare-gas overlayers.

On the other hand, dissociative attachment reactions (4) and (5) are dependent on the yield and energy distribution of the secondary electrons [Fig. 9(a) and 9(b)]. In Sec. IV D we discuss the influence of the rare-gas overlayer on the secondary electrons.

Note that primary electrons are expected to cause desorption of rare-gas atoms as well as neutral F species. One might argue that a depletion of the rare-gas film could increase the measured F ion yield. However, the electron fluence used is low, $<2\times10^{13}$ cm$^{-2}$, and the total Xe desorption cross section is only $3\times10^{-19}$ cm$^2$.[24,25] Hence we exclude any significant depletion in the rare-gas overlayer occurring during measurement. (We find the F ion yields to be independent of electron fluence in the fluence range used.)

Another question is whether the same electron that causes the ESD of a F ion can also disturb the rare-gas film, e.g., through excitation or ionization of a rare-gas atom. The ex-

citation of the rare-gas atom can result in nuclear motion of the rare-gas atom. However, as we discussed earlier,[9] the large mass difference between the ESD fluorine ion and the rare-gas atoms leads to no significant motion of the rare-gas atoms during the time it takes the fluorine ion to desorb through the overlayer. Hence, although we do not exclude the possibility of fluorine ion desorption through a disturbed film, it seems improbable that this affects the measured parameters significantly.

### B. Geometric ball model

In Fig. 11(a) we present a possible geometric ball model of 1 ML Kr with the fcc(111) structure on the 1-ML $PF_3$/Ru(0001) surface. The Kr atoms interact only weakly with the $PF_3$ layer, as can be seen from the small difference in desorption temperature of the TDS monolayer peak (47 K) and multilayer peak (43 K) (Fig. 1). This indicates that the binding energy of a Kr atom in the first monolayer is only slightly larger than the binding energy of a Kr atom in the multilayer, and suggests that Kr forms an incommensurate close-packed complete layer on the substrate with a nearest-neighbor distance very close to that of bulk krypton (4.0 Å).[26,27] As seen in Fig. 11(a), the nearest-neighbor distance of Kr is slightly smaller than the $PF_3$ nearest-neighbor distance.

The nearest-neighbor distance in bulk xenon is slightly larger than that of Kr, 4.3 Å.[26,27] In Fig. 11(b) we depict a geometric ball model. Based on an argument similar to that for Kr, we assume that Xe also forms an incommensurate close-packed complete first layer on $PF_3$/Ru(0001). The subsequent rare-gas layers are assumed to grow in a layer-by-layer fashion (*A*-*B*-*C*-*A*...).

### C. Attenuation model

Assuming that a rare-gas film grows in a layer-by-layer fashion, it is expected that the attenuation of an ion signal in the rare-gas film would be linear within one layer, provided that the attenuation collision radii do not overlap.[12] If the ions penetrate several layers of the rare-gas solid, the envelope of the transmission curve, composed of several linear segments between integral monolayer coverage points, is given by an exponential function.[28] In our earlier study, since the $O^+$ ions penetrate several layers of the rare-gas solid, we have derived the $O^+$ attenuation cross sections using an exponential equation which is based on a continuum model in a solid:

$$\Phi = \Phi_0 \exp(-N\sigma d) \tag{7}$$

where $\Phi$ and $\Phi_0$ are the total ion flux reaching the detector and the total ion flux desorbing from the surface, respectively, $N$ the rare-gas number density, $d$ is the rare-gas film thickness, and $\sigma$ the attenuation cross section.

For the very large attenuation cross-section limit of this model ($\sigma \gg 1/Nd$), the attenuation within one layer is expected to be exponential regardless of the overlayer growth modes (layer-by-layer or statistical growth). This exponential attenuation within one layer results from the overlapping of the effective interaction area of neighboring overlayer atoms (molecules) with increasing coverage. [Note that if the effective interaction area is smaller than the atomic diameter of the overlayer atoms, little or no overlapping of the effective interaction area of neighboring overlayer atoms (molecules) occurs with increasing coverage.] In the transmission of ~7-eV $O^+$ ions through $H_2O$, we have explained the strong exponential attenuation of the $O^+$ yield in the $H_2O$ overlayer having a thickness $<1$ ML based on this model;[12] with increasing $H_2O$ coverage the effective interaction areas of neighboring $H_2O$ molecules overlap, because the effective interaction area ($R \approx 5.3$ Å; $\sigma \approx \pi R^2$; $\sigma \approx 9\times10^{-15}$ cm$^2$) is much larger than the molecular size ($R_{H_2O} \approx 1.45$ Å).

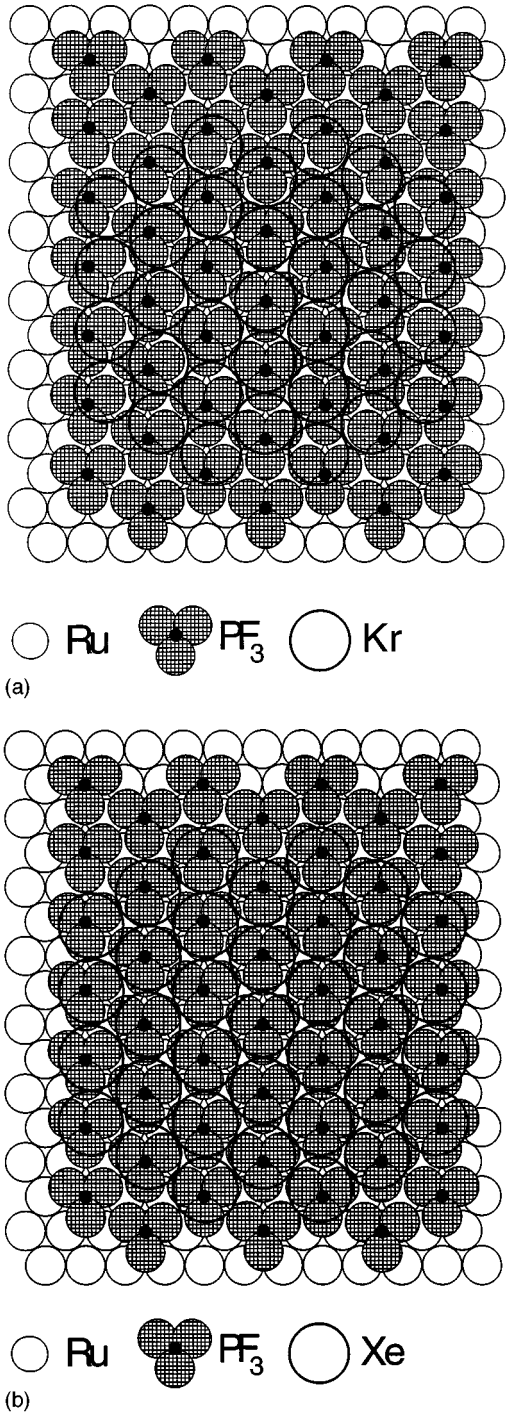


FIG. 11. Geometric ball model for 1 ML of (a) Kr and (b) Xe adsorbed on 1-ML $PF_3$/Ru(0001). The circles are based on atomic radii (Refs. 26 and 27). See text for explanations.

For layer-by-layer growth, if the atomic diameter of the overlayer atoms is larger than the measured cross section, the attenuation within one layer is expected to be linear. In the present study, the $F^+$, $F^-$, and $F_2^-$ signals are found to be attenuated substantially by Kr or Xe films $\leq 1$ ML thick (0–1 ML for $F^+$ and $F_2^-$ and 1–2 ML for $F^-$). The measured attenuation cross sections indicate that with increasing coverage the effective interaction areas of neighboring Kr (Xe) atoms overlap by only a small amount, if at all, because the measured attenuation collision radii derived from the attenuation cross sections ($\sigma=\pi R^2$) (for example, $R\approx 2.1$ Å for $KrF^+$, $R\approx 2.6$ Å for $XeF^+$, $R\approx 1.8$ Å for $KrF^-$, and $R\approx 2.2$ for $XeF^-$) are comparable to the van der Waals atomic radii of Kr (~2.0 Å) and Xe (2.17 Å).[26] Therefore, the attenuation of the $F^+$, $F^-$, and $F_2^-$ signals are not readily described by an exponential model through a single monolayer. We use a linear attenuation model to derive the attenuation cross section of the $F^+$, $F^-$, and $F_2^-$ signals in the Kr and Xe overlayers.

As discussed in Sec. III D, the comparison of the $F^-$ attenuation cross section with the $F_2^-$ attenuation cross section indicates that the $F^-$ and $F_2^-$ attenuation cross sections in the rare-gas films depend strongly on the rare-gas film thickness, because the sizes of these ions are relatively large. In our earlier study of $O^+$ transmission through rare-gas (Kr and Xe) films, we have found that the $O^+$ attenuation cross sections for films thinner than 2 ML are independent of the rare-gas coverage.[9] This is well correlated with the size of an $O^+$ ion; the diameter of $O^+$ (~0.44 Å) is so small that a change in the channel size in going from 1 to 2 ML does not affect the $O^+$ attenuation cross sections. However, upon completion of the third rare-gas layer the channels are closed, and the desorbing $O^+$ ions interact with the rare-gas atoms much more effectively. Hence the measured attenuation cross sections of $O^+$ for films thicker than 2 ML are larger those for $<2$ ML.[9,11]

In Ref. 14, we have derived the $F^-$ attenuation cross section in the Xe coverage range 1.5–3.5 ML using an exponential attenuation model. Note that the attenuation cross section of $F^-$ in Xe ($\sim 5.1\times 10^{-15}$ cm$^2$) derived using the exponential model[14] is considerable higher than the attenuation cross section ($1.5\times 10^{-15}$ cm$^2$) between 1 and 2 ML derived using the linear model in this paper (Sec. III B.) We suggest that this is a consequence of the thickness dependence of the $F^-$ attenuation cross section in Xe, but more measurements are needed to verify this point.

### D. Attenuation of $F^+$ in Kr and Xe

In a previous paper,[11] we analyzed the transmission behavior of $O^+$ ions through thin rare-gas films. The transmission behavior could be understood both by using molecular-dynamics simulations, and in terms of a simple geometrical model. Since both models used only elastic scattering for describing the interaction between $O^+$ and the rare-gas film, and because the model calculations agreed so well with the experimental data,[9,11] it was concluded that inelastic effects could be neglected for the transmission of $O^+$ through Kr and Xe in this approach.

It appears worthwhile to try to discuss the results of the present experiments in terms of elastic scattering. Unfortunately, a $F^+$ rare-gas potential—either measured or calculated—does not seem to be available. This might be due to the fact that the ionization potential of F (17.43 eV) is larger than that of Xe (12.13 eV),[27] and that the ground state of the ionic molecule $(FXe)^+$ is a spin singlet, while asymptotically for large distances, according to Hund's rule, the system $Xe\text{-}F^+$ is a spin triplet. As a consequence, the $F^+$-Xe interaction is described by a (highly) excited state well above the $(FXe)^+$ ground state, with the ''wrong'' symmetry; this renders the quantum chemical calculation of the potential curve relevant for the present work quite intricate. This lack of information precludes the possibility of performing molecular-dynamics simulations. Hence we shall present only an elastic-scattering analysis in the spirit of the geometric model published previously.[11]

For perpendicular ion emission ($F^+$ center beam) and integral monolayer coverage, the model assumes the rare-gas atoms to be spheres—or rather discs—centered on a hexagonal lattice with spacing $a=d/\sqrt{2}$, where $d$ is the lattice constant of the bulk rare-gas crystal. Ions are transmitted through the film only if their starting point lies in the open area not covered by the discs. For perpendicular emission, the extension of this model to fractional coverage $x$ is obvious. The model has one parameter, the disc radius $r_0$. It represents the impact parameter in a $F^+$ rare-gas collision for which a laboratory scattering angle of 90° occurs.

In Figs. 12(a) and 12(b), the results of this geometric model are plotted for Kr and Xe, and compared to the result of the experiments presented above. The fit parameter has a value of $r_0/a=0.56$ (0.66), which corresponds to 2.1 Å (2.9 Å) for Kr (Xe) films [using crystallographic data for $a$ (Ref. 26)]. It is seen that the agreement of the model with the experimental data is satisfactory. The disc radius is rather large, in particular if it is compared with the corresponding radius for $O^+$-Xe (Kr) interaction, which is 1.4 Å.[11] This is discussed at the end of Sec. IV E. Note that the disc radius is also larger than the van der Waals atomic radius, 2.0 Å for Kr and 2.17 Å for Xe.[26] Using the disc radius (2.1 Å for $F^+$-Kr and 2.9 Å for $F^+$-Xe interactions), we can derive geometric attenuation cross sections of $\sim 1.4\times 10^{-15}$ cm$^2$ for Kr and $\sim 2.6\times 10^{-15}$ cm$^2$ for Xe. The calculated cross sections are in very good agreement with the measured cross sections ($\sim 1.4\times 10^{-15}$ cm$^2$ for Kr and $\sim 2.2\times 10^{-15}$ cm$^2$ for Xe).

In the case of oblique emission of $F^+$ (off-normal beams), the application of a geometric model is considerably more complicated due to the shadowing of Xe atoms. Furthermore, the details of the interaction potential become more important in this case, since now even particles which have been scattered by an angle larger than 90° can be emitted from the surface, if they hit the rare-gas atom on the ''upper'' side—i.e., the side opposing the surface. When hitting it on the ''lower'' side—the one facing the surface—only very glancing collisions will not lead to reflection. Thus we assume that these two effects tend to cancel, and that the $F^+$ rare-gas scattering can be described by the same effective value of $r_0$ as in the case of perpendicular emission. However, we note that this makes the rigorous application of the geometric model doubtful.

We calculate the open area fraction for general emission angles using a Monte Carlo technique of area integration. 10 000 test particles are launched along straight trajectories with starting points randomly distributed over the surface

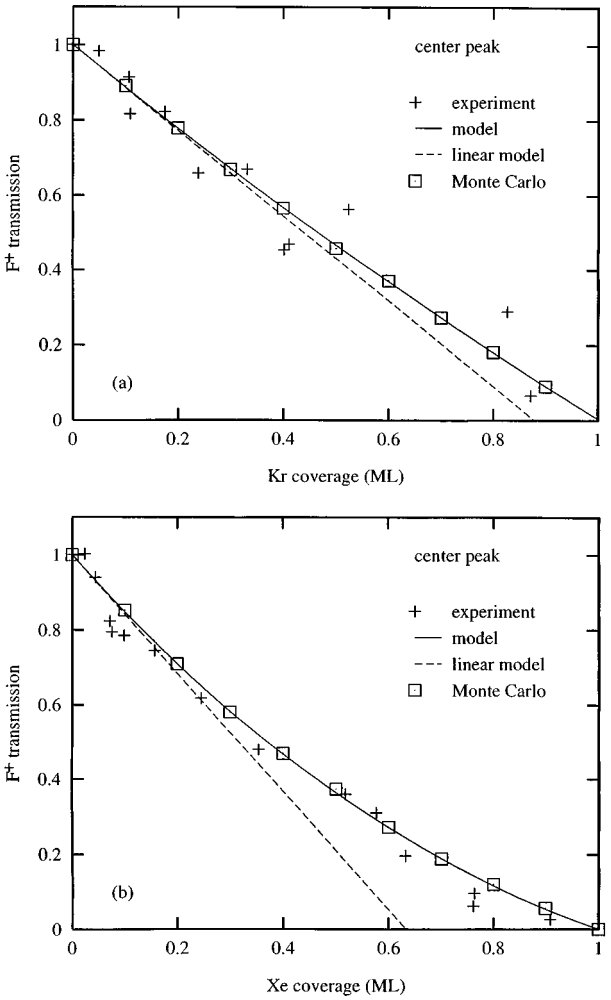


FIG. 12. Results of the geometric model discussed in Sec. IV D for $F^+$ transmission in the normal direction as a function of rare-gas coverage for (a) Kr and (b) Xe. The results of the model agree well with the experimental data. The linear model agrees with the experimental data only for low coverages, as expected.

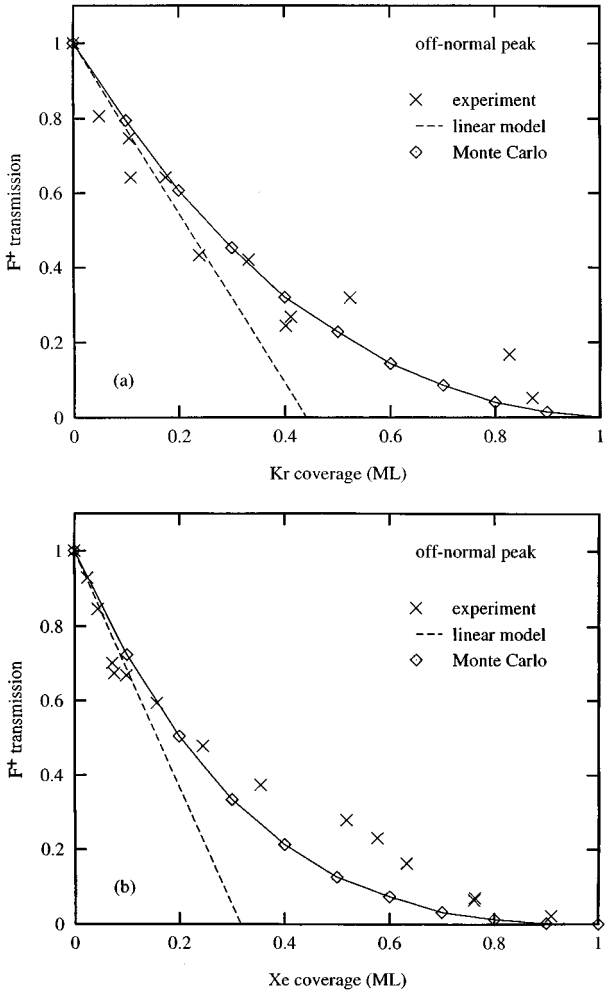


FIG. 13. Results of the geometric model discussed in Sec. IV D for $F^+$ transmission in the off-normal (60°) direction as a function of rare-gas coverage for (a) Kr and (b) Xe. The results of the model agree well with the experimental data. The linear model agrees with the experimental data only for low coverages, as expected.

unit cell. Each trajectory is checked for blocking by rare-gas atoms. The fraction of unblocked trajectories obtained in this way is (apart from statistical error) just the open area fraction. We check the code by comparison to analytical results for perpendicular emission; as Fig. 12 shows, we obtain good agreement. In Fig. 13 we plot the Monte Carlo results of the off-normal transmission yields assuming an emission angle of $\theta=60°$. We note that here the same value of $r_0/a$ as that determined for the perpendicular $F^+$ emission was used. The agreement of experiment and model is satisfactory.

A linear analysis for small coverages $x$, where shadowing can be neglected, can be performed for arbitrary emission angles $\theta$, and for the transmission yield we obtain

$$Y=1-\frac{2\pi}{\sqrt{3}}\left(\frac{r_0}{a}\right)^2\frac{x}{\cos\theta}. \tag{8}$$

Here the attenuation appears as a product of the rare-gas density $\sqrt{2}/a^3$, the geometric cross section $\pi r_0^2$, and the path $\sqrt{2/3}xa/\cos\theta$ covered by the $F^+$ ion in the rare-gas film. (The thickness of 1 ML is $\sqrt{2/3}a$). The linearized results have been included in Figs. 12 and 13.

It may seem surprising that the differences in attenuation of normal and off-normal beams are not larger. For large penetration depths (multilayers) one might expect that the attenuation cross section scales with the cosine of the polar angle of desorption. However, the $F^+$ ions are completely attenuated by only 1 ML of Kr or Xe, and in this thickness range the attenuation should not follow the cosine law.

So far we have derived disc radii for $F^+$/Kr and $F^+$/Xe, and have concluded that the attenuation of $F^+$ in the rare gases is stronger than the attenuation of $O^+$ in Kr and Xe having a thickness $\leqslant 2$ ML. Hence we consider that besides elastic scattering as an attenuation mechanism for $F^+$, one-electron charge transfer might be another attenuation mechanism for $F^+$.

The reactions

$$F^+ + Kr \rightarrow F + Kr^+ \tag{9}$$

and

$$F^+ + Xe \rightarrow F + Xe^+ \tag{10}$$

are exothermic by 3.42 and 5.29 eV, based on gas phase values for ionization potentials (F: 17.42 eV; Kr: 14.00 eV; Xe: 12.13 eV).[26] It is commonly understood that at very low collision energies (<10 eV), exothermic charge-transfer reactions can have rather high cross sections ($10^{-15}$–$10^{-14}$ $cm^2$), and are therefore likely to occur.[29] However, Rapp and Francis[30] concluded that even exothermic charge-transfer cross sections are small if the exothermicity is large [this is the case in (9) and (10)]. At the present time we cannot make a definite decision on whether charge transfer is the dominant attenuation mechanism. It is likely to occur, but its importance is unclear.

The relatively small contribution of large angle scattering for $F^+$ (which, in contrast, is substantial for $F^-$, Fig. 5) appears to be in agreement with the charge-transfer model: $F^+$ ions which collide with rare-gas atoms such that the collision leads to a significant change in angle of $F^+$ (small impact parameter) are neutralized, and therefore cannot be detected with our ion detector. This point requires further investigation.

### E. Increase in $F^-$ upon passage through Kr and Xe

To understand the increase in $F^-$ at rare-gas coverages up to 1 ML (Figs. 6 and 7) we consider charge-transfer reactions in the rare-gas films, the effect of the rare-gas overlayer on the initial ESD processes, and the effect of the rare gases on ESD final-state effects.

#### *Charge-transfer reactions in the rare-gas films*

We must consider the possibility that the increase of $F^-$ is a product of the collision of other desorbing species, such as $F^+$, F, or $F_2{}^-$ with rare-gas atoms in the overlayer film. (Note that although we cannot detect ground-state neutrals with our experimental setup, it can be expected that neutral F atoms are among the desorption products.) First, we consider the process

$$F + RG \rightarrow F^- + RG^+. \tag{11}$$

The energy defect $\Delta E$ is the difference between the ionization potential IP of the RG and the electron affinity EA of F. (Note that the endothermicity is based on the unscreened value of the electron affinity of F and the atomic ionization potentials of Kr and Xe.) Using tabulated values of IP(Kr) =14.00 eV, IP(Xe)=12.1 eV, and EA(F)=3.4 eV,[26,27] we obtain an energy defect for $F^-$-Kr of 10.6 eV and for $F^-$-Xe of 8.7 eV. Reaction (11) is highly endothermic, and therefore energetically not possible under the conditions of our experiment (the kinetic energy of a neutral F is expected to be below 5 eV).

Another possible source of $F^-$ is $F^+$. We consider the following mechanism:

$$F^+ + RG \rightarrow F^- + RG^{2+}. \tag{12}$$

Using a value of IP(F) of 17.4 eV, and values of energies to remove two electrons from Kr of 38.56 eV and from Xe of 33.3 eV,[26] reaction (12) is found to be strongly endothermic by 17.8 eV for Kr and 12.5 eV for Xe, so that this process is not likely to produce a $F^-$ ion with sufficient kinetic energy to desorb.

Finally, we consider $F_2{}^-$ as a source for $F^-$ production. It is also attenuated within the first monolayer of Kr or Xe, and could produce $F^-$ according to

$$F_2{}^- + RG \rightarrow F^- + F + RG. \tag{13}$$

This reaction may be energetically possible since the bond strength in the $F_2$ molecule is only 1.6 eV,[27] which is probably the same order of magnitude as the kinetic energy of $F_2{}^-$. However, the $F_2{}^-$ yield is only ~10% of the $F^-$ yield from the clean $PF_3$ surface; if the initial $F_2{}^-$ yield is not affected by the presence of the rare-gas overlayer, then Eq. (13) cannot explain the >2-fold increase in $F^-$. Also, note that $F_2{}^-$ does not decrease immediately at very low coverages, at which the $F^-$ yield already increases.

Therefore, we conclude that a charge-transfer collision in the film leading to formation of $F^-$ is not likely to be the dominant mechanism causing the strong increase in $F^-$ yield. In the following we investigate whether the Xe overlayer can lead to an increase in production of $F^-$.

#### *Initial ESD processes*

In Sec. IV A we describe the dominant mechanisms of formation of $F^+$, $F^-$, and $F_2{}^-$. We have pointed out that the primary (300 eV) electrons do not lose a significant amount of energy in the rare-gas film, so that the initial ESD processes in reactions (2) and (3) are not significantly affected by the presence of the rare-gas overlayer. However, the dissociative attachment reactions (4) and (5) are initiated by low-energy electrons, which are most likely secondary electrons from the substrate. We now discuss how the secondary electron yield from the substrate may be influenced by the rare-gas overlayer.

Secondary electrons are emitted from the Ru substrate following collisions of primary electrons. On their way into vacuum, they are transmitted through the $PF_3$ layer. We expect that in the presence of a rare-gas overlayer, some secondary electrons can be reflected back toward the substrate and hence be transmitted through the $PF_3$ layer multiple times, thereby increasing the rate of dissociative attachment to $PF_3$. However, the reflection coefficient for secondary electrons scattered from rare-gas atoms is low;[31,32] although the reflection of secondary electrons from the rare-gas layer may lead to a slight increase in production of $F^-$ through reaction (4), it cannot solely explain the strong increase observed in $F^-$.

We also consider that the primary electrons can create secondary electrons in the rare-gas film, which then can contribute to the dissociative attachment reactions (4) and (5). However, since the ionization cross sections of Kr or Xe by 300-eV electrons are only $2.8\times10^{-16}$ and $4\times10^{-16}$ $cm^2$, each primary electron will produce $\ll 1$ secondary electron; hence this process can only make a minor contribution to the increase in the $F^-$ yield, at least within the first rare-gas ML. This is in agreement with our findings that the secondary electron emission from 1 ML rare gas on $PF_3$/Ru is not significantly higher that for $PF_3$/Ru [Figs. 9(a) and 9(b)]. Hence we concentrate in the following section on how the rare-gas overlayer may influence final-state effects in ESD of $F^-$ from $PF_3$.

### *ESD final-state effects*

There are two main factors that influence the escape probability of ESD ions from a surface: the image force attraction[33] and neutralization[34] (ESD final-state effects). The image force attracts a desorbing ion toward the surface; for ions desorbing with large polar angles (off-normal) the image interaction can inhibit the ion's escape from the surface. The other factor is neutralization of the ion with the surface upon desorption. This will be the focus of the following discussion.

The ion survival probability $P$; which is the probability that the ion desorbs without neutralization, is given by

$$P = \exp\left[ -\int_{Z_0}^{\infty} R(z(t))dt \right], \tag{14}$$

where $z(t)$ is the time-dependent ion-surface separation in a classical trajectory approach, and $Z_0$ is the initial ion-surface separation. $R(z)$ is the reneutralization rate and depends on the ion-surface distance.

If adsorption of a rare-gas layer affects the lifetime of a final state that leads to ion desorption from the chemisorbed $PF_3$ layer, the initial ion yield from $PF_3$ could be influenced. As discussed in Sec. IV B, Kr and Xe interact with the $PF_3$ layer very weakly. Hence we do not expect that the presence of a very weakly interacting rare-gas overlayer has a strong effect on the lifetime of the final states of electronically excited $PF_3$. Even a layer of $H_2O$, which interacts more strongly with $PF_3$ than the rare-gas layers, does not seem to affect the initial ESD ion desorption probability from $PF_3$.[35] In addition, evidence that a rare-gas layer has little or no influence on the initial ESD of $O^+$ from oxidized W has been reported previously.[9,10]

It has been shown that a change in the work function of a surface can lead to a change in the desorption yield of negative ions from that surface. Joyce *et al.*[20] investigated the coadsorption of potassium with $PF_3$/Ru(0001). Potassium leads to a decrease in the work function of the surface, and this decrease has been suggested to cause a decrease in the neutralization probability $R(z)$ of the desorbing $F^-$ with the surface. This served as an explanation for the experimental observation that the $F^-$ yield from $PF_3$/Ru(0001) increases upon coadsorption of potassium.

We illustrate this situation in Fig. 14: there can be a neutralization of the desorbing negative ion $F^-$ with the surface through electron transfer $R_e$, from the electron affinity level $\varepsilon_a$, into an unoccupied state of the substrate. If the work function were strongly decreased (e.g., by $\sim$2 eV), then the affinity level would be on the same level as, or below, the occupied levels of the substrate, and the neutralization probability would be decreased significantly; this could lead to an enhanced $F^-$ yield.

We have shown in Fig. 9(c) that the adsorption of rare gas on the $PF_3$/Ru(0001) surface leads to a decrease of the work function; however, the decrease is very small ($\sim$0.07 eV/RG ML). This makes it unlikely that the change in the work function alone can explain the strong increase in the $F^-$ yield.

We suggest that the main reason for the enhancement of $F^-$ is dielectric screening of the desorbing $F^-$ from the surface caused by the rare-gas film. The neutralization of a negative ion with a surface is very high at ion-surface distances where the electron affinity level of the negative ion and the unoccupied levels of the metal cross.[36] The ion-surface distance ($z$), where the neutralization is most efficient, may be at a value $z$ which lies outside of the first monolayer of the rare gas film. This means that most of the desorbing $F^-$ ions pass through the rare-gas monolayer without significant neutralization; the neutralization probability of the $F^-$ ion outside the rare-gas monolayer may be reduced as compared to the probability in the absence of the rare-gas film, because the electrons have to tunnel through the rare-gas film (Fig. 14), which increases the electron tunneling barrier due to dielectric screening. Preliminary calculations by Nordlander show that this effect may very well explain the strong increase in the $F^-$ yield upon rare-gas adsorption.[37] In conclusion, we believe that the dominant factor causing an increase in the $F^-$ yield is dielectric screening through the rare-gas film, but other factors such as a decrease in the work function or a small increase in the $F^-$ production may also contribute to the increase.

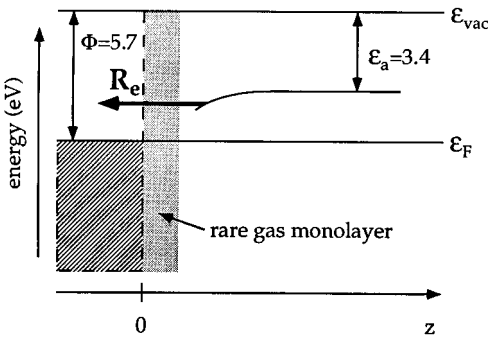


FIG. 14. Schematic of the energy levels of $F^-$ relative to the substrate Fermi level. Φ: work function of $PF_3$/Ru(0001); $\varepsilon_a$; electron affinity of $F$; $\varepsilon_{vac}$: vacuum level; $\varepsilon_F$: Fermi level; $R_e$: negative ion neutralization distance. Also shown is the approximate geometric position of 1 ML of rare gas.

### F. Attenuation and deflection of $F^-$ in Kr and Xe

After having discussed a mechanism that explains the increase in the total $F^-$ yield by the rare-gas overlayer, we now suggest a model to explain the strong change in the angular distribution of the $F^-$ ions with increasing rare-gas coverage, and the attenuation of the $F^-$ ions in the rare-gas films. The $F^-$ ions which desorb initially on trajectories with a polar angle of $\sim$60° are elastically scattered toward the surface normal, which results in the broad angular distribution centered around the surface normal. Upon completion of 1 ML of Kr or Xe, nearly all ions are found in the broad normal distribution. The reason for this scattering lies in the structure of the rare-gas solids: Bulk rare-gas solids are known to have a fcc structure, which for the (111) direction corresponds to a layering of *A-B-C-A*... . Based on arguments made in Sec. IV B, we assume that rare-gas films also grow on the substrate $PF_3$/Ru(0001) in a fcc(111) structure. As we have pointed out in an earlier paper,[9] this structure exhibits channels perpendicular to the surface until completion of the third layer. In order to escape through the rare-gas film from the surface, the $F^-$ ions have to change their polar angle of desorption and follow one of the perpendicular channels.

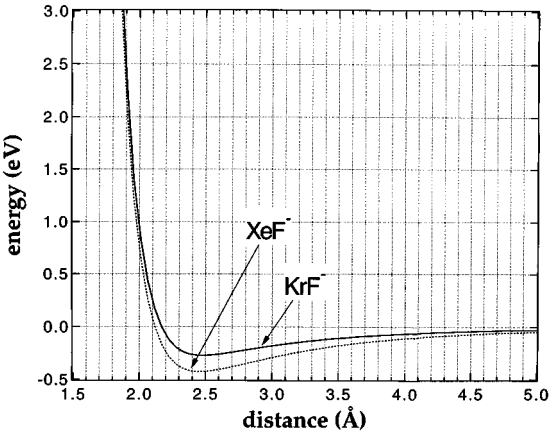


FIG. 15. Interaction potentials for the systems $KrF^-$ and $XeF^-$. The data are obtained from the paper by Mansky and Flannery (Ref. 39).

An important condition for the ion to be able to escape from the surface as an ion is that it does not change its charge state in the collision, i.e., that it does not neutralize. We can understand this by considering the following reactions:

$$F^- + Kr \rightarrow F + Kr^- \tag{15}$$

and

$$F^- + Xe \rightarrow F + Xe^-. \tag{16}$$

These reactions are endothermic by 3.1 and 3.0 eV [the electron affinity of F is 3.4 eV, and that of solid Kr (Xe) is 0.3 (0.4) eV].[38] This means that even if all of the peak kinetic energy of $F^-$ ($\sim$1 eV) were used for reactions (15) or (16), the reaction would still not be likely. This is the reason why ions can survive collisions with impact parameters so small that the ions change their angle by $\sim$60°.

Another important condition for the escape of the scattered ions from the surface is that their kinetic energy has to be sufficiently large so that they are not recaptured by the image interaction or neutralized with the surface. Using a classical hard-sphere ball model, we calculate the energy loss of 2 eV $F^-$ in a collision with a Kr (Xe) atom that leads to a change in angle of 60° to be only 0.4 eV (0.28 eV). This demonstrates that due to the large rare-gas atom mass, most ions still have enough kinetic energy to escape the surface.

By analogy to our analysis in Ref. 11, we determine the backscattering cross section and the energy loss from the $(FKr)^-$ and $(FXe)^-$ potentials published by Mansky and Flannery[39] (reproduced in Fig. 15). They are depicted in Figs. 16 and 17. The backscattering cross sections and energy loss (stopping power) are very similar to those obtained previously for $O^+Kr$ and $O^+Xe$.[11] One of the differences between the $O^+$ and $F^-$ experiment is the kinetic energy of the ion: $\sim$7 eV for $O^+$ vs 1 eV for $F^-$. For $F^-$ transmission as compared to $O^+$ transmission, this slightly increases the angular scattering of the ions, but decreases the stopping power of the ions in the rare-gas film. Hence this analysis shows that the $F^-$ transmission through Kr and Xe should be ''comparable'' to the $O^+$ transmission.

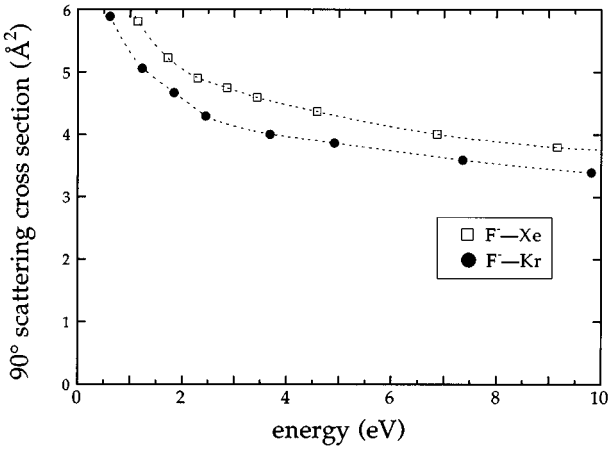


FIG. 16. Backscattering cross sections in binary collision approximation of $F^-$ ions in rare-gas films.

Earlier, for the case of $O^+$ transmission through Kr and Xe, we concluded that the dominant attenuation mechanism is elastic scattering, and that inelastic effects (such as charge transfer) do not contribute significantly to the attenuation.[9,10] By analogy, and based on the analysis given above, we suggest here that the attenuation of $F^-$ in Kr and Xe is also dominated by elastic scattering. This is supported by the observation of large angle scattering (Fig. 5). We do not completely exclude the possibility that inelastic effects may contribute to the $F^-$ attenuation, but they are probably not dominant.

### G. Attenuation of $F_2^-$ in Kr and Xe

We suggest that the reasons for the increase in $F_2^-$ in the presence of Kr or Xe are the same as those discussed in Sec. IV E for the increase in $F^-$, i.e., mainly changes in the final-state effects for $F_2^-$ desorption.

It is not surprising that all $F_2^-$ ions are suppressed upon completion of 1 ML of rare-gas overlayer. Although the changes in the final-state effects of desorption may lead to a decrease in the neutralization probability of $F_2^-$, the molecule is too large to escape through the channels in the rare-gas film. The van der Waals radius of F is 1.35 Å, which

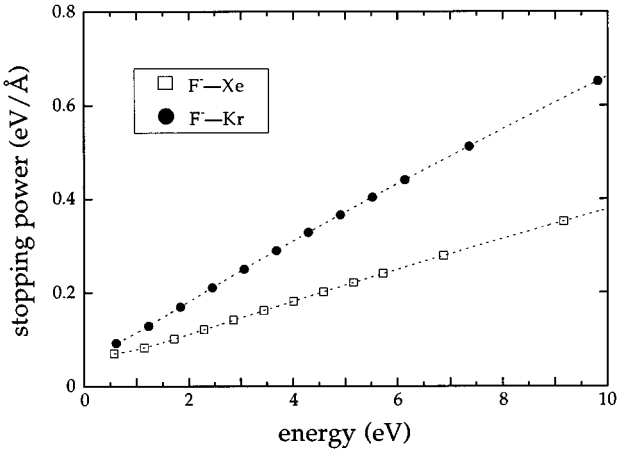


FIG. 17. Stopping power $dE/dx$ in the binary collision approximation of $F^-$ ions traversing a rare-gas films.

means that the van der Waals diameter of $F_2^-$ is $>3.7$ Å (the single-bond covalent radius of F is $\sim 0.64$ Å),[19] much larger than the channel size in the rare-gas film.

Note that elastic collisions of $F_2^-$ with rare-gas atoms can also lead to a significant reduction in kinetic energy: Using again a classical hard-sphere ball model we calculate as an example the energy loss of a 2-eV $F_2^-$ in a collision with a Kr (Xe) atom that leads to a change in angle of 60° to be 0.8 eV (0.5 eV). This means that not all ions may have enough kinetic energy to escape the surface.

Note that since $F_2^-$ formation from $PF_3$ by electron bombardment involves a rearrangement of $PF_3$, we cannot rule out the possibility of electronic quenching of the formation of $F_2^-$ by Kr and Xe. This initial-state effect caused by adsorption of Kr (Xe) overlayers may also reduce the $F_2^-$ yield significantly.

## V. SUMMARY AND CONCLUSIONS

We can summarize our results as follows:

(1) $F^+$ ions are attenuated nearly completely by $\sim 1$ ML of Kr or Xe. For the normal $F^+$ beam, we derive the attenuation cross sections of $(1.4\pm0.4)\times10^{-15}$ cm$^2$ for Kr and $(2.2\pm0.6)\times10^{-15}$ cm$^2$ for Xe, in the coverage range $<1$ ML.

(2) Adsorption of 1 ML of Kr or Xe on top of $PF_3$/Ru(0001) leads to an increase in $F^-$ yield and to a change in the $F^-$ angular distribution.

(3) $F^-$ ions are attenuated in Kr with a cross section of $(1.1\pm0.6)\times10^{-15}$ cm$^2$, and in Xe with $\sim(1.5\pm0.4)\times10^{-15}$ cm$^2$.

(4) $F_2^-$ ions are attenuated completely by 1 ML of Kr or Xe.

We suggest a model in which the ions are attenuated by elastic scattering and by charge transfer. $F^-$ undergoes mainly elastic scattering, while $F^+$ may also be attenuated by one-electron charge-transfer processes. The increase in the $F^-$ yield for rare-gas films $<1$ ML thick is attributed to a decrease in the neutralization probability of the desorbing ions with the surface due to dielectric screening, and is therefore a specific effect of the system studied which has two interfaces, Kr(Xe)/$PF_3$ and $PF_3$/Ru(0001).

This study is part of a series of investigations of the transmission of low-energy ions through ultrathin films; these measurements are directly related to the depth of origin of secondary ions.[9,10,12–14,40] In all of the studies so far we have attributed the attenuation of low-energy ions in thin films to either elastic scattering or charge transfer. In most cases, charge transfer seems to be an important attenuation mechanism (besides elastic scattering) when the charge-transfer reaction is exothermic. The structure of the film has been found to play an important role for the attenuation and for the trajectories of the ions traversing the film; we have found evidence of channeling of the ions in the films.[9] The penetration depth of ions in thin films has been found to range from a fractional monolayer to 6 ML.

## ACKNOWLEDGMENTS

P.K. and H.M.U. are grateful to W. Meyer and P. Sebald for discussions and helpful advice on the calculation of $F^+$ rare-gas potentials. This work has been supported in part by the National Science Foundation, Grant No. CHE-9408367.

*Present address: McKinsey & Co., Kurfürstendamm 185, D-10707 Berlin, Germany.

†Author to whom correspondence should be addressed.

[1] H. Massey and H. Gilbody, *Electronic and Ionic Impact Phenomena* (Clarendon, Oxford, 1974).

[2] J. B. Hasted, *Physics of Atomic Collisions* (Elsevier, New York, 1972).

[3] R. E. Johnson, *Energetic Charged-Particle Interactions with Atmospheres and Surfaces* (Springer-Verlag, Berlin, 1990).

[4] P. Sigmund, A. Oliva, and G. Falcone, Nucl. Instrum. Methods **194**, 541 (1982).

[5] M. Vicanek, J. J. J. Rodriguez, and P. Sigmund, Nucl. Instrum. Methods Physics Phys. Res. Sect. B **36**, 124 (1989).

[6] P. Sigmund *et al.*, Nucl. Instrum. Methods Phys. Res. Sect. B **36**, 110 (1989).

[7] J. W. Burnett, J. P. Biersack, D. M. Gruen, B. Jørgensen, A. R. Kraus, M. J. Pellin, E. L. Schweitzer, J. T. Yates, Jr. and C. E. Young, J. Vac. Sci. Technol. A **6**, 2064 (1988).

[8] M. F. Dumke, T. A. Tombrello, R. A. Weller, R. M. Housley, and E. H. Cirlin, Surf. Sci. **124**, 407 (1983).

[9] N. J. Sack, M. Akbulut, and T. E. Madey, Phys. Rev. B **51**, 4585 (1995).

[10] N. J. Sack, M. Akbulut, and T. E. Madey, Phys. Rev. Lett. **73**, 794 (1994).

[11] P. Klein, M. Vicanek, and H. Urbassek, Phys. Rev. B **51**, 4597 (1995).

[12] M. Akbulut, N. J. Sack, and T. E. Madey, J. Chem. Phys. **103**, 2202 (1995).

[13] U. Diebold and T. E. Madey, Phys. Rev. Lett. **72**, 1116 (1994).

[14] N. J. Sack, M. Akbulut, and T. E. Madey, Surf. Sci. **334**, L695 (1995).

[15] N. J. Sack, L. Nair, and T. E. Madey, Surf. Sci. **310**, 63 (1994).

[16] A. L. Johnson, S. A. Joyce, and T. E. Madey, Phys. Rev. Lett. **61**, 2578 (1988).

[17] H. Schlichting and D. Menzel, Surf. Sci. **272**, 27 (1992).

[18] T. E. Madey, H.-S. Tao, L. Nair, U. Diebold, S. M. Shivaprasad, A. L. Johnson, A. Poradzisz, N. D. Shinn, J. A. Yarmoff, V. Chakarian, and D. Shuh, in *Desorption Induced by Electronic Transitions DIET V*, edited by A. R. Burns, E. B. Stechel, and D. R. Jennison (Springer-Verlag, Berlin, 1993), p. 182.

[19] L. Pauling, *General Chemistry* (Dover, New York, 1970).

[20] S. A. Joyce, C. Clark, V. Chakarian, D. H. Shuh, J. A. Yarmoff, T. E. Madey, P. Nordlander, B. Maschoff, and H.-S. Tao, Phys. Rev. B **45**, 14 264 (1992).

[21] M. Akbulut, T. E. Madey, L. Parenteau, and L. Sanche, J. Chem. Phys. (to be published).

[22] T. E. Madey, Science **234**, 316 (1986).

[23] L. J. Kieffer, At. Data **1**, 19 (1969).

[24] Q. J. Zhang and R. Gomer, Surf Sci. **109**, 567 (1981).

[25] Q. J. Zhang, R. Gomer, and S. R. Bowman, Surf. Sci. **129**, 535 (1983).

[26] C. Kittel, *Introduction to Solid State Physics* (Wiley, New York, 1986).

[27] R. C. Weast, *CRC Handbook of Chemistry and Physics* (CRC Press, Boca Raton, FL, 1988).
[28] H. Lüth, *Surfaces and Interfaces of Solids* (Springer-Verlag, Berlin, 1993).
[29] F. Linder, in *Electronic and Atomic Collisions*, edited by H. B. Gilbody, W. R. Newell, F. H. Read, and A. C. Smith (Elsevier, Amsterdam, 1988), p. 287.
[30] D. Rapp and W. E. Francis, J. Chem. Phys. **37**, 2631 (1962).
[31] S. K. Jo and J. M. White, J. Chem. Phys. **94**, 5761 (1991).
[32] T. L. Gilton, C. P. Dehnbostel, and J. P. Cowin, J. Chem. Phys. **91**, 1937 (1989).
[33] Z. Miskovic, J. Vukanic, and T. E. Madey, Surf. Sci. **141**, 285 (1984).
[34] Z. Miskovic, J. Vukanic, and T. E. Madey, Surf. Sci. **169**, 405 (1986).
[35] M. Akbulut, N. J. Sack, and T. E. Madey, Phys. Rev. Lett. **75**, 3414 (1995).
[36] P. Nordlander and N. D. Lang, Phys. Rev. B **44**, 13 681 (1991).
[37] P. Nordlander (private communication).
[38] N. Schwentner, E.-E. Koch, and J. Jortner, *Electronic Excitations in Condensed Rare Gases*, Springer Tracts in Modern Physics (Springer-Verlag, Berlin, 1985).
[39] E. J. Mansky and M. R. Flannery, J. Chem. Phys. **99**, 1962 (1993).
[40] N. J. Sack, M. Akbulut, and T. E. Madey, Nucl. Instrum. Methods Phys. Res. B **90**, 451 (1994).